AD-A169 515 THE ASPERITY AND MATERIAL PARAMETERS IN THERMOMECHANICAL CRACKING DUE TO..(U) NEW MEXICO UNIV ALBUQUERQUE DEPT OF MECHANICAL ENGINEERING F D JU 1/1

UNCLASSIFIED FEB 86 ME-136(86)ONR-233-3 N00014-84-K-0252 F/G 20/11 NL

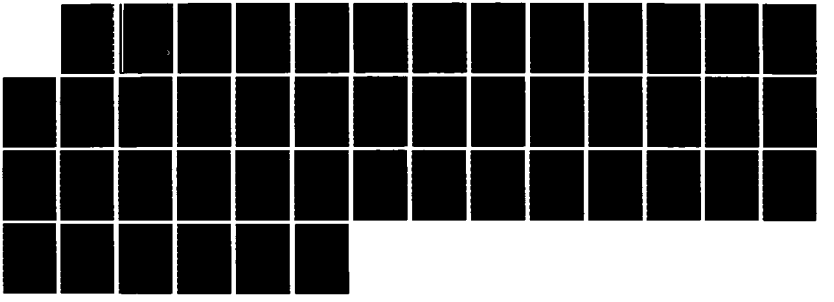

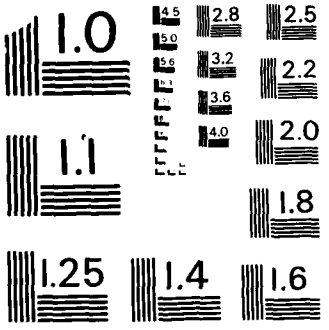

(12)

THE UNIVERSITY OF NEW MEXICO
COLLEGE OF ENGINEERING

BUREAU OF ENGINEERING RESEARCH

THE ASPERITY AND MATERIAL PARAMETERS IN THERMOMECHANICAL CRACKING DUE TO MOVING FRICTION LOAD

by
Frederick D. Ju
The University of New Mexico

Technical Report
ME-136(86)ONR-233-3

Work Performed Under Contract No. ONR-N00014-84-K-0252

February 1986

UNLIMITED DISTRIBUTION

Technical Report

on

THE ASPERITY AND MATERIAL PARAMETERS IN THERMOMECHANICAL CRACKING DUE TO MOVING FRICTION LOAD

by

Frederick D. Ju

Department of Mechanical Engineering

The University of New Mexico

Albuquerque, New Mexico 87131

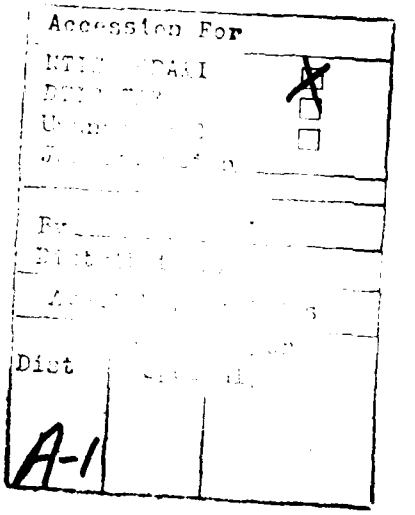

Report No. ME-136(86)ONR-233-3

Work Performed Under Contract No. ONR-N00014-84-K-0252

February 1986

ABSTRACT

When an asperity traverses at a relatively high speed over the surface of a medium, the resulting friction force in the contact zone may cause a "hot spot" that would lead eventually to "heat-checking" or thermomechanical cracking in the medium. The asperity traversing speed, the load distribution of the asperity over the contact area and the relative dimensions of the contact area all affect the stress state in the medium, thus the initiation of fracture therein. Moreover, the mechanical and the thermal properties of the medium also play significant roles in the susceptibility of themomechanical cracking ~~of the medium,~~ thus wear of the friction surface. In the present paper, it is shown that by assuming a uniform distribution of the load over the contact zone, the predicted stress level could be 40% less than that of a non-uniform distribution of an equal total load. While the shape of the contact area does not affect the stress level, its size does. For the same average pressure, increasing the size in the direction of asperity travel raises the stress level; while increasing the aspect ratio (relatively increasing the length normal to the traversing direction) lowers the stress level. In the limit of an infinite aspect ratio (a plane strain model), less than 20% of the stress level at the aspect ratio of one results. The multifacet influence of asperity speed manifests in rate of thermal energy input and in the thermal layer thickness, which determines the magnitude of thermal stress and the location of fracture initiation. In the mechanical and the thermal properties of the medium material, higher coefficient of Coulomb friction and higher Young's modulus, as expected, lead to higher stress. But higher Poisson's ratio does not significantly increase the stress. High thermal expansion coefficient and low thermal capacity are well known to be the source of high thermal stress. The result

bears out their effect in thermomechanical cracking. However, thermal capacity and thermal conductivity jointly influence the thermal field through the thermal diffusivity, which occurs in the governing differential equation. The report demonstrates that the thermal diffusivity is indeed a derived thermal parameter. It is the values of thermal capacity and the thermal conductivity individually that determines the thermal field, thus the stress field that leads to thermomechanical cracking of the wear medium.

TABLE OF CONTENTS

List of Figures

NOMENCLATURE

a	Asperity characteristic dimension, the half width of the rectangular contact area in the direction of traverse or radius of the circular contact area.
b	Half length of the rectangular contact area perpendicular to the direction of traverse.
c	Specific heat
E	Young's Modulus
k	Thermal conductivity
$p(x_1,x_2)$	Load distribution
P_o	Average pressure over the contact area
P_e	Peclet Number (= Va/k)
q_o	Heat flux through the contact area
R_i	Traction over the contact area in the x_i direction
t	Aspect ratio (b/a) or time coordinate
T	Temperature field
$\{u_i\}$	Displacement field
V	Traverse speed of asperity ($-x_1$ direction)
$\{x_i\}$	Coordinates fixed to the moving asperity
∂_i	Partial derivative with respect to x_i coordinate
α	Coefficient of thermal expansion
ϕ	Dimensionless temperature field (= $Tk/q_o a$)
κ	Thermal diffusivity
λ	Lame coefficient
μ	Lame coefficient, modulus of rigidity
μ_f	Coulomb coefficient of friction
ν	Poisson's ratio
ρ	Mass density

σ_{ij}	Stress field
σ_{ij}^{M}	Mechanical Stress field
σ_{ij}^{T}	Thermal stress field
σ_{I}	Maximum combined thermomechanical principal stress
$\{\xi,\eta,\zeta\}$	Dimensionless coordinates ($= x_i/a$)
ζ_m	Dimensionless depth of maximum thermal gradient
$(\bar{\ })$	Fourier transform of ( )

1.0 INTRODUCTION

In some mechanical systems, mating surfaces are pressed against each other and undergo relative sliding motion, which may occur with dry friction either by design or inadvertently through normal operation. Had the pressure been evenly distributed according to design, the service life of the device would not be a serious problem even at a high rubbing speed. However, it is well known that the actual contact area may only be a small fraction of the nominal area at the design interface [1]. Burton [2] considered 10^{-4} as a possible areal ratio (the ratio between the actual contact area and the nominal area at the design interface). In other words, a low nominal design pressure may result in a very high interfacial pressure, thus a very high dry frictional force in the actual contact area. Experiments have demonstrated such high friction, and the resulting extremely high local temperature, called a "hot spot" [3,4]. The hot spot is considered one of the causes of frictional cracking, or "heat checking" [5]. It suffices to assume that the localization of contact area is due to some form of asperities, from thermoelastic instability or impurities, which may be fixed to any of the mating surfaces or may precess with respect to both. Based on a model of asperities fixed to one mating surface and tneir excitation, thermo-mechanical actions, on the other hard mating surface, Ju and Huang [6,7] developed a three dimensional theory of thermo-mechanical cracking. In the general theory, the complicated solutions were left in the expressions of Fourier transform. Numerical solutions were obtained for material properties similar to those of Stellite III. It was shown that, for a conservative areal ratio of 10^{-3}, a 240 kPa (35 psi) design pressure could result in a 240 MPa (35000 psi) asperity pressure. At this pressure, a moderate Coulomb coefficient of 0.5 and an asperity traversing speed of 10

mps (400 ips) would lead to thermo-mechanical cracking, initiating at a depth of one-tenth asperity size, approximately 100 μm deep. A general review of related works is referred to [7]. The present report shall study the asperity and the material parameters which influence the thermo-mechanical stress state in the medium which lead to heat checking.

1.1 Mathematical Model and Parameters

The phenomenon of thermomechanical cracking, as observed from experiments and operational damages, is seen to associate with relatively hard materials; such as cast iron, Stellite III and the likes. The plastic wear and surface shear are restricted in a very thin surface layer, Blau [9] and Ruff and Blau [10]. Thermo-mechanical cracking could very well initiate at sub-surface region, where the material behavior is essentially thermo-elastic. The governing differential equation are the thermoelastic Navier's equation and the uncoupled Fourier equation, respectively

$$(\lambda+\mu)\partial_{ij}u_j + \mu\partial_{jj}u_i = \rho\ddot{u}_i + (3\lambda+2\mu)\alpha\partial_i T, \tag{1}$$

and

$$k\,\partial_{ii}\,T = \dot{T}, \tag{2}$$

where $\partial_i = \partial/\partial x_i$, (λ,μ) are the Lame's coefficients, ρ is the mass density, α is the coefficient of thermal expansion and κ the thermal diffusivity. The indices in the subscript i,j,k, = 1,2,3 and the summation convention are used for all repeated indices of roman minuscules. The stress field $\{\sigma_{ij}\}$ can be expressed in terms of the thermoelastic Hookian Law:

$$\sigma_{ij} = \lambda\partial_k u_k\delta_{ij} + \mu(\partial_j u_i + \partial_i u_j) - (3\lambda + 2\mu)\alpha T\delta_{ij}, \tag{3}$$

where δ_{ij} is the Kronecker delta. The coordinates, $\{x_i\}$, in Equations (1-3), are material coordinates; that is, they are fixed to the wear

material over which the asperity traverses. The field variables, $\{u_i\}$ and T, as evidenced in Equations (1,2), are defined in (x_i,t). In other words, time is an explicity variable. The moving boundary conditions are also time dependent. We can now restate our mathematical model as follows. The size of the asperities under consideration are of the order of 1 mm; the thickness of the hard material that was acted on is at least an order of magnitude larger. Hence, the material is adequately represented by a half space with the asperity traversing over the surface boundary at a uniform speed (V) as shown in Figure 1. At high speed traversing, the high temperature and surface yield due to the excitation are subgranular. If the region of consideration is away from such subgranular layer, the half space region is basically elastic and subjected to brittle fracture. For the present purpose, the material can be considered as homogeneous and isotropic without local flaws. In the analytical formulation, with respect to the material reference frame (fixed to the half space material), the field variables $\{u_i,T\}$ will have local time variation. Hence, the problem is transient. However, by taking into consideration the uniform properties of the materials, asperity motions and loadings, we can justify the invariant states of the field variables. In other words, with respect to a convective reference frame (fixed to the asperity thus moving relative to the material), the analytical formulation becomes "steady state"; that is, there is no explicit time variable. The coordinates shown in Figure 1 are convective such that x_1 is oriented along and opposite to the asperity-traversing direction; x_3 is perpendicular to the boundary surface into the material; and x_2 is parallel to the surface but perpendicular to the traversing direction. The governing differential equations for the displacement field $\{u_i\}$ and the temperature field (T) in the material referring to the convective coordinates, the dynamic thermoelastic Navier's equation (1) and the uncoupled Fourier law (2), become:

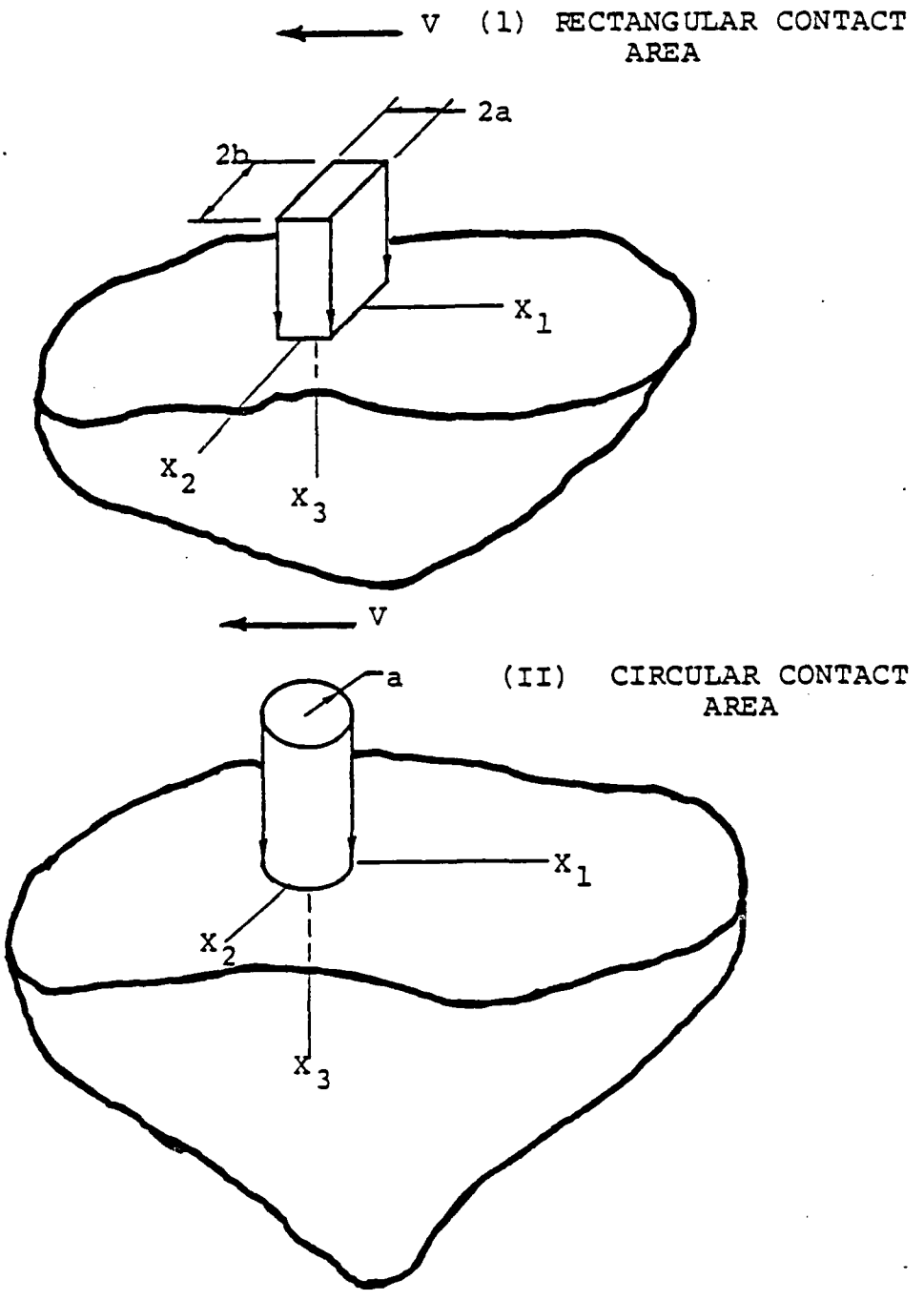

Figure 1. Asperity excitation over the wear medium.

$$(\lambda + \mu)\partial_{ij}u_k + \mu\partial_{jj}u_i = \rho V^2\partial_{II}u_i + (3\lambda + 2\mu)\alpha\partial_i T, \tag{4}$$

$$k\partial_{ii}T = V\partial_I T. \tag{5}$$

The Equations (4,5) are only implicitly time dependent. The boundary conditions in terms of the convective coordinates are also time-independent. On the surface

$$\sigma_{3i} = - R_i, \tag{6}$$

and

$$k\partial_3 T = - VR_1, \tag{7}$$

where the tractions are: $R_2 = 0$, $R_3 = P(x_1,x_2)$ and $R_1 = \mu_f P(x_1,x_2)$ in the contact region and zero everywhere, $P(x_1,x_2)$ is the asperity pressure, μ_f is the coefficient of Coulomb friction and k is the thermal conductivity. Without loss of generality, the mating surface and the non-contact wear surface are assumed to be adiabatic.* The regularity conditions for the stress and temperature fields hold at infinity; that is, at $x_i x_i = \infty$,

$$\sigma_{ij} = 0, \tag{8}$$

and

$$T = 0. \tag{9}$$

From the governing differential equations (4,5) and the boundary conditions, Equations (6,7), we can thus delineate the parameters as those characterizing the asperity and those the material. The groups of parameters are listed as follows

---

* The thermal energy loss across the free surface by convection is small generally. Since the maximum temperature gradient occurs at the immediate vicinity of the moving asperity, the heat loss by convection will not alter significantly on the criterion for thermo-mechanical cracking.

Table I

Asperity parameters

V	Asperity traversing speed
$P(x_1,x_2)$	Asperity pressure
a	Asperity contact area width (in the traversing direction)
b	Contact area length
	Contact area shape

Table II

Material parameters

λ, μ or E,ν	Mechanical constitutive coefficients
ρ	Mass density
μ_f	Coefficient of Coulomb friction
α	Coefficient of thermal expansion
κ	Thermal diffusivity
k	Thermal conductivity

The present report will study the effect of these parameters.

1.2 Analytical Solutions

For general solutions of Equations (4,5), Fourier transforms of co-ordinates (x_1x_2) are used, resulting in ordinary differential equations in x_3; that is

$$\bar{f}(\bar{x}_1,\bar{x}_2,x_3) = \mathcal{F}[f(x_i)] = \frac{1}{2\pi}\int_{-\infty}^{\infty}\int f(x_i)\exp[i(\bar{x}_1x_1+\bar{x}_2x_2)]dx_1dx_2, \quad (8)$$

where, and in the sequel, $(\bar{\ })$denotes the Fourier transform $\mathcal{F}[(\ )]$. The temperature fields are obtained in the transformed space and are employed directly as input to the transformed differential equation of Equation (4). The inverse transform of special cases are carried out by numerical methods. The numerical method itself is checked with the solutions of temperature field, which can be alternatively obtained by the Green's function solution [8].

The non-homogeneous differential equation (4), subjected to nonhomogeneous boundary condition (6), is solved by dividing the stress and the displacement fields $\{\sigma_{ij}, u_i\}$ into two portions

$\{\sigma_{ij}^M, u_i^M\}$ and $\{\sigma_{ij}^T, u_i^T\}$ such that

$$u_i = u_i^M + u_i^T, \tag{9}$$

$$\sigma_{ij} = \sigma_{ij}^M + \sigma_{ij}^T. \tag{10}$$

The individual displacement and stress components are related following the thermoelastic Hookian Law, Equation (3), as:

$$\sigma_{ij}^M = \lambda \partial_k u_k^M \delta_{ij} + \mu \left(\partial_j u_i^M + \partial_i u_j^M\right), \tag{11}$$

$$\sigma_{ij}^T = \lambda \partial_k u_k^T \delta_{ij} + \mu \left(\partial_j u_i^T + \partial_i u_j^T\right) - (3\lambda + 2\mu)\alpha T \delta_{ij}. \tag{12}$$

The set $\{\sigma_{ij}^M, u_i^M\}$ is required to satisfy the homogeneous differential equation but nonhomgeneous boundary condition; that is, in the region,

$$(\lambda + \mu)\partial_{ij} u_j^M + \mu \partial_{jj} u_i^M = \rho V^2 \partial_{11} u_i^M, \tag{13}$$

and on the boundary,

$$\left.\begin{aligned} \sigma_{3i}^M &= -R_i, \text{ on the surface;} \\ \sigma_{ij}^M &= 0, \quad \text{at } x_k x_k = \infty. \end{aligned}\right\} \tag{I4}$$

The set $\{\sigma_{ij}{}^T, u_i{}^T\}$ is to satisfy the non-homogeneous differential equation but homogeneous boundary condition; that is, in the region

$$(\lambda + \mu)\partial_{ij}u_j{}^T + \mu\partial_{jj}u_i{}^T = \rho V^2\partial_{11}u_i{}^T + (3\lambda + 2\mu)\alpha\partial_i T, \tag{15}$$

and on the boundary,

$$\left.\begin{aligned} &\sigma_{3i}{}^T = 0, \quad \text{on the surface;} \\ &\sigma_{ij}{}^T = 0, \quad \text{at } x_k x_k = \infty. \end{aligned}\right\} \tag{16}$$

The mathematical delineation, for convenience of solution, essentially in the physical sense separates the stress and the displacement fields into two parts. One $\{\sigma_{ij}{}^M, u_i{}^M\}$ results from the mechanical excitation of the asperity; those are the traversing normal pressure and frictional traction. Another $\{\sigma_{ij}{}^T, u_i{}^T\}$ is solely the consequence of temperature field or rather its gradient $\{\partial_i T\}$, resulted from the heat input due to frictional energy loss rate. They are respectively called the mechanical portion and the thermal portion of the solutions. It is noticed from the Fourier equation (5,7), that the temperature field is itself the result of the friction force $\mu_f P$. Friction, therefore, directly affects the mechanical portion as well as the thermal portion of the solutions. The relative dominance of each portion, as evidence from the thermal boundary condition Equation (7), depends on the traversing speed V of the asperity.

The general solutions of the mechanical portion in the Fourier transformed expressions as given in [6] are:

$$2\mu F\ \bar{u}_1^M = (i\bar{x}_1 n_3 \bar{R}_3 - \bar{x}_1^2 n_2 \bar{R}_1 - \bar{x}_1 \bar{x}_2 n_2 \bar{R}_2)\ e^{-n_1 x_3} - \Big\{ i\bar{x}_1 n_1 n_2 \bar{R}_3 -$$

$$- \Big[\frac{\bar{x}_2^2}{n_2} (n_3 - 2n_1 n_2) + n_2 n_3 \Big] \bar{R}_1 + \frac{\bar{x}_1 \bar{x}_2}{n_2} (n_3 - 2n_1 n_2)\ \bar{R}_2 \Big\}\ e^{-n_2 x_3},$$

$$2\mu F\ \bar{u}_2^M = (i\bar{x}_2 n_3 \bar{R}_3 - \bar{x}_1 \bar{x}_2 n_2 \bar{R}_1 - \bar{x}_2^2 n_2 \bar{R}_2)\ e^{-n_1 x_3} - \Big\{ i\bar{x}_2 n_1 n_2 \bar{R}_3 +$$

$$+ \frac{\bar{x}_1 \bar{x}_2}{n_2} (n_3 - 2n_1 n_2)\ \bar{R}_1 - \Big[\frac{\bar{x}_1^2}{n_2} (n_3 - 2n_1 n_2) + n_2 n_3 \Big] \bar{R}_2 \Big\}\ e^{-n_2 x_3},$$

$$2\mu F\ \bar{u}_3^M = (n_1 n_3 \bar{R}_3 + i\bar{x}_1 n_1 n_2 \bar{R}_1 + i\bar{x}_2 n_1 n_2 \bar{R}_2)\ e^{-n_1 x_3} -$$

$$- [n_1 (\bar{x}_1^2 + \bar{x}_2^2)\ \bar{R}_3 + i\bar{x}_1 n_3 \bar{R}_1 + i\bar{x}_2 n_3 \bar{R}_2]\ e^{-n_2 x_3}, \qquad (17)$$

$$F\,\bar{\sigma}_{11}^{M} = \bar{B}\,[(\bar{x}_1^2 + \bar{x}_2^2 - n_1^2) + \bar{x}_1^2]\,e^{-n_1 x_3} - \{\bar{x}_1^2 n_1 n_2 \bar{R}_3 +$$

$$+ i\bar{x}_1\,[\bar{x}_2^2 N_2 + n_2 n_3]\,\bar{R}_1 - i\bar{x}_1^2 \bar{x}_2 N_2 \bar{R}_2\}\,e^{-n_2 x_3},$$

$$F\,\bar{\sigma}_{22}^{M} = \bar{B}\,[(\bar{x}_1^2 + \bar{x}_2^2 - n_1^2)\,K + \bar{x}_2^2]\,e^{-n_1 x_3} - \{\bar{x}_2^2 n_1 n_2 \bar{R}_3 -$$

$$- i\bar{x}_1 \bar{x}_2^2 N_2 \bar{R}_1 + i\bar{x}_2\,[\bar{x}_1^2 N_2 + n_2 n_3]\,\bar{R}_2\}\,e^{-n_2 x_3},$$

$$F\,\bar{\sigma}_{33}^{M} = \bar{B}\,[(\bar{x}_1^2 + \bar{x}_2^2 - n_1^2)\,K - n_1^2]\,e^{-n_1 x_3} +$$

$$+ n_2\,[(\bar{x}_1^2 + \bar{x}_2^2)\,n_1 \bar{R}_3 + i n_3\,(\bar{x}_1 \bar{R}_1 + \bar{x}_2 \bar{R}_2)]\,e^{-n_2 x_3},$$

$$F\,\bar{\sigma}_{12}^{M} = \bar{x}_1 \bar{x}_2 B\,e^{-n_1 x_3} - \{\bar{x}_1 \bar{x}_2 n_1 n_2 \bar{R}_3 + \tfrac{1}{2}\,\bar{x}_2\,[n_2 n_3 -$$

$$- (\bar{x}_1^2 - \bar{x}_2^2)\,N_2]\,\bar{R}_1 + \tfrac{1}{2}\,\bar{x}_1\,[n_2 n_3 + (\bar{x}_1^2 - \bar{x}_2^2)\,N_2]\,\bar{R}_2\}\,e^{-n_2 x_3},$$

$$F\,\bar{\sigma}_{23}^{M} = -i\bar{x}_2 n_1 \bar{B}\,e^{-n_1 x_3} + \{i\bar{x}_2 n_1\,(\bar{x}_1^2 + \bar{x}_2^2 + n_2^2)\,\bar{R}_3 -$$

$$- 2\bar{x}_1 \bar{x}_2 n_1 n_2 \bar{R}_1 - [\bar{x}_1^2 N_1 + n_3\,(n_2^2 + \bar{x}_2^2)\,\bar{R}_2\}\,e^{-n_2 x_3}/2,$$

$$F\,\bar{\sigma}_{31}^{M} = -i\bar{x}_1 n_1 \bar{B}\,e^{-n_1 x_3} + \{i\bar{x}_1 n_1\,(\bar{x}_1^2 + \bar{x}_2^2 + n_2^2)\,\bar{R}_3 -$$

$$- [\bar{x}_2^2 N_1 + n_3\,(n_2^2 + \bar{x}_1^2)]\,\bar{R}_1 - 2\bar{x}_1 \bar{x}_2 n_1 n_2 \bar{R}_2\}\,e^{-n_2 x_3}/2, \qquad (18)$$

where $n_r = (\bar{x}_s \bar{x}_s - M_r^2 \bar{x}_1^2)^{1/2}$,

$n_3 = \bar{x}_s \bar{x}_s - \frac{1}{2} M_2^2 \bar{x}_1^2$,

$M_r = V/c_r$, $c_1^2 = (\lambda + 2\mu)/\rho$, $c_2^2 = \mu/\rho$,

$F = n_3^2 - n_1 n_2 \bar{x}_s \bar{x}_s$,

$N_1 = n_3 - 2n_1 n_2$, $N_2 = N_1/n_2$,

$$K = \lambda/2\mu = \nu/(1 - 2\nu)$$

$$\bar{B} = n_3\bar{R}_3 + in_2\bar{x}_s\bar{R}_s, \qquad r,s = 1,2,$$

$$\bar{R}_i = \mathcal{F}[R_i].$$

The expressions of the mechanical portion are quite general, applicable for any traction $\{R_i\}$. Specifically for the problem of asperity excitation, R_3 is the asperity pressure $P(x_1,x_2)$, R_1 is the asperity friction $\mu_f P$ and $R_2 = 0$ in the contact area of the surface and zero everywhere else on the surface. By taking R_1 and R_3 serparately, the computation can be much simplified and also can afford a comparison of stress fields as effected by normal pressure and frictional force.

The temperature field in the Fourier transformed expression is:

$$\bar{T} = e^{-\omega x_3}\{[C_1\cos(\theta x_3) + C_2\sin(\theta x_3)]\,\bar{P}_1 + [C_3\cos(\theta x_3) + C_4\sin(\theta x_3)]\,\bar{P}_2\}, \tag{19}$$

where

$$C_1 = \frac{-2\omega^2 + in}{2\omega(\omega^2 + \theta^2)},$$

$$C_2 = \frac{2\theta^2 + in}{2\theta(\omega^2 + \theta^2)},$$

$$C_3 = \frac{-n - i2\omega^2}{2\omega(\omega^2 + \theta^2)},$$

$$C_4 = \frac{-n + i2\theta^2}{2\theta(\omega^2 + \theta^2)},$$

$$\theta = \left[\frac{(s^4 + n^2)^{1/2} - s^2}{2}\right]^{1/2},$$

$$\omega = \left[\frac{(s^4 + n^2)^{1/2} - s^2}{2}\right]^{1/2},$$

$$s^2 = \bar{x}_1^2 + \bar{x}_2^2, \qquad n = -V\bar{x}_1/\kappa,$$

and $$\bar{P}_1 + i\bar{P}_2 = V\bar{R}_1/k.$$

The temperature fields for individual cases are left in the Fourier transformed expression as the excitation to the transformed differential equation of the thermal portion $\{\sigma_{ij}^T, u_i^T\}$ of the thermoelastic Navier's equation (15,16). The temperature fields, in inverse transformed expressions, are used as a double check of the numerical procedure against the Green's function solutions and also serve to correlate the temperature gradient with the maximum tensile stress.

The expressions of the thermal component $\{\sigma_{ij}^T, u_i^T\}$ are very complex, that it is rendered necessary to resort to numerical methods in inverse Fourier transforms for individual values of parameters. The Fourier transformed expressions of thermal components are given as

$$\bar{u}_r^T = \frac{\bar{x}_r}{\bar{x}_2}(h_1 + h_2x_3)\, e^{-sx_3} +$$

$$+ \frac{a_3\bar{x}_r}{2a_1\omega\theta}[G\cos(\theta x_3) + H\sin(\theta x_3)]\, e^{-\omega x_3}, \quad r = 1,2,$$

$$\bar{u}_3^T = -\frac{i}{a_2\bar{x}_2}[a_2 s(h_1 + h_2x_3) + (a_2 + 2)h_2]\, e^{-sx_3} +$$

$$+ \frac{a_3}{2a_1\omega\theta}[G_3\cos(\theta x_3) + H_3\sin(\theta x_3)]\, e^{-\omega x_3}, \qquad (20)$$

where $$H = \frac{-(n + i2\omega^2)\,\bar{P}_1 + (2\omega^2 - in)\,\bar{P}_2}{2\omega(\omega^2 + \theta^2)} = i(C_1\bar{P}_1 + C_3\bar{P}_2),$$

$$G = \frac{(n - i2\theta^2)\,\bar{P}_1 + (2\theta^2 + in)\,\bar{P}_2}{2\theta(\omega^2 + \theta^2)} = -i(C_2\bar{P}_1 + C_4\bar{P}_2),$$

$$G_3 = -i(\omega G - \theta H), \qquad H_3 = -i(\omega H - \theta G),$$

$$a_1 = a_4 + 2 = 2(1 - \nu)/(1 - 2\nu),$$

$$a_2 = a_4 + 1 = 1/(1 - 2\nu),$$

$$a_3 = (3a_4 + 2)\alpha = 2\alpha(1 + \nu)/(1 - 2\nu),$$

$$a_4 = \lambda/\mu = 2\nu/(1 - 2\nu).$$

$$h_1 = \frac{a_3\bar{x}_2}{2a_1a_2s^2\omega\theta}\,[a_1s\theta\, H + (s^2 - a_1s\omega + a_1\theta^2)\, G],$$

and $$h_2 = \frac{a_3\bar{x}_2}{2a_1s\omega\theta}\,[-s\theta\, H - (s^2 - s\omega + a_1\theta^2)\, G].$$

The Fourier transformed expressions of the thermal stress field are:

$$\frac{\bar{\sigma}_{11}^{T}}{\mu} = i\left[\,(-b_1H + b_2G)\, e^{-\omega x_3} + (-b_3H + b_4G)\, e^{-sx_3}\,\right],$$

$$\frac{\bar{\sigma}_{22}^{T}}{\mu} = i\left[\,(-b_5H + b_6G)\, e^{-\omega x_3} + (-b_7H + b_8G)\, e^{-sx_3}\,\right],$$

$$\frac{\bar{\sigma}_{33}^{T}}{\mu} = i\left[\,(-b_9H + b_{10}G)\, e^{-\omega x_3} + (b_{11}H - b_{12}G)\, e^{-sx_3}\,\right],$$

$$\frac{\bar{\sigma}_{12}^{T}}{\mu} = i\bar{x}_1\bar{x}_2\left[\,(-b_{13}H + b_{14}G)\, e^{-\omega x_3} + (-b_{15}H + b_{16}G)\, e^{-sx_3}\,\right],$$

$$\frac{\bar{\sigma}_{23}^{T}}{\mu} = -\bar{x}_2\left[\,(b_{17}H - b_{18}G)\, e^{-\omega x_3} - (b_{19}H - b_{20}G)\, e^{-sx_3}\,\right],$$

$$\frac{\bar{\sigma}_{31}^{T}}{\mu} = -\bar{x}_1\left[\,(b_{17}H - b_{18}G)\, e^{-\omega x_3} - (b_{19}H - b_{20}G)\, e^{-sx_3}\,\right], \qquad (21)$$

where

$$b_1 = \frac{-a_3}{a_1\omega\theta}\,[2\omega\theta\,\cos(\theta x_3) - \bar{x}_1^{\,2}\,\sin(\theta x_3)],$$

$$b_2 = \frac{-a_3}{a_1\omega\theta}\,[\bar{x}_1^{\,2}\,\cos(\theta x_3) + 2\omega\theta\,\sin(\theta x_3)],$$

$$b_3 = \frac{a_3}{\omega}\left(\frac{\bar{x}_1^{\,2}}{a_2 s} + \frac{a_4 s}{a_1 a_2} - \frac{\bar{x}_1^{\,2} x_3}{a_1}\right),$$

$$b_4 = \frac{a_3}{a_1\omega\theta}\left[\frac{a_1\omega - s}{a_2 s}\,\bar{x}_1^{\,2} + \frac{a_4(s\omega - s^2)}{a_2} + (s - \omega)\,\bar{x}_1^{\,2} x_3\right],$$

$$b_5 = \frac{-a_3}{a_1\omega\theta}\,[2\omega\theta\,\cos(\theta x_3) - \bar{x}_2^{\,2}\,\sin(\theta x_3)],$$

$$b_6 = \frac{-a_3}{a_1\omega\theta}\,[\bar{x}_2^{\,2}\,\cos(\theta x_3) + 2\omega\theta\,\sin(\theta x_3)],$$

$$b_7 = \frac{a_3}{\omega}\left(\frac{\bar{x}_2^{\,2}}{a_2 s} + \frac{a_4 s}{a_1 a_2} - \frac{\bar{x}_2^{\,2} x_3}{a_1}\right),$$

$$b_8 = \frac{a_3}{a_1\omega\theta}\left[\frac{a_1\omega - s}{a_2 s}\,\bar{x}_2^{\,2} + \frac{a_4(s\omega - s^2)}{a_2} + (s - \omega)\,\bar{x}_2^{\,2} x_3\right],$$

$$b_9 = \frac{-a_3 s^2}{a_1\omega\theta}\,\sin(\theta x_3),$$

$$b_{10} = \frac{a_3 s^2}{a_1\omega\theta}\,\cos(\theta x_3),$$

$$b_{11} = -\frac{a_3 s^2}{a_1\omega}\,x_3,$$

$$b_{12} = \frac{a_3 s^2}{a_1\omega\theta}\,[1 + (s - \omega)\,x_3],$$

$$b_{13} = \frac{a_3}{a_1\omega\theta} \sin(\theta x_3),$$

$$b_{14} = -\frac{a_3}{a_1\omega\theta} \cos(\theta x_3),$$

$$b_{15} = \frac{a_3}{\omega}\left(\frac{1}{a_2 s} - \frac{x_3}{a_1}\right),$$

$$b_{16} = \frac{a_3}{a\ \omega\theta}\left[\ \frac{a_1\omega - s}{a_2 s} + (s - \omega)\ x_3\ \right],$$

$$b_{17} = \frac{a_3}{a_1\omega\theta}\left[-\theta \cos(\theta x_3) + \omega \sin(\theta x_3)\right],$$

$$b_{18} = \frac{-a_3}{a_1\omega\theta}\left[\omega \cos(\theta x_3) + \theta \sin(\theta x_3)\right],$$

$$b_{19} = \frac{a_3}{a_1\omega}\left(-1 + s x_3\right),$$

$$b_{20} = \frac{a_3}{a_1\omega\theta}\left[-\omega + s(\omega - s)\ x_3\right].$$

Equations (17,18,20,21) are the general solutions of $\{\sigma_{ij}{}^{M},\ u_i{}^{M}\}$ and $\{\sigma_{ij}{}^{T},\ u_i{}^{T}\}$ in their Fourier tranformed expressions. With given excitation conditions: $\{R_i, V\}$. The inverse transform can be carried out numerically. The numerical technique was reported by Ju and Huang in [6]. The effects of individual parameters are therefore analyzed through specific numerical variations of their values.

2.0 ASPERITY PARAMETERS

The asperity parameters involve those excitation-related, the actual pressure and its traversing speed (P,V), and those related to the geometry of the contact area, its width in the direction of traverse, it length and its shape (a, b, contact are shape). The excitation-related parameters are principally design oriented. Yet the actual pressure and its distribution in the contact area have to be determined empirically. The contact area configuration is not readily known to be controllable by design. However, studies of these parameters are important in analysis of wear resistance, to promote reliabililty in design. The studies will provide the unstanding in adequacy of analysis by using a two-dimensional model or by assuming an uniform distribution of pressure (thus friction) in the contact region.

2.1 Excitation Parameters

The traversing speed of the asperity (V) influences both the convective acceleration term, Equations (13,15), and the thermal input, Equation (7). It is readily conceivable that at low rubbing speed the mechanical portion of the stress dominates. In the limit at zero traversing speed, there may still be mechanical field; but the thermal field becomes trivial. At high speed asperity excitation the thermal field prevails. The present report addresses specifically the latter case.

At high speed excitation, the temperature is high near the surface, and the thermal stress is compressive as a result of constraint against thermal expansion. At below surface layer, where the temperature field has high gradient, the interparticle constraint thus creates high tensile stresses, which at unfavorable loading could lead to crack initiation through cohesive failure. The phenomenon is illustrated in Figure 2, showing the stress

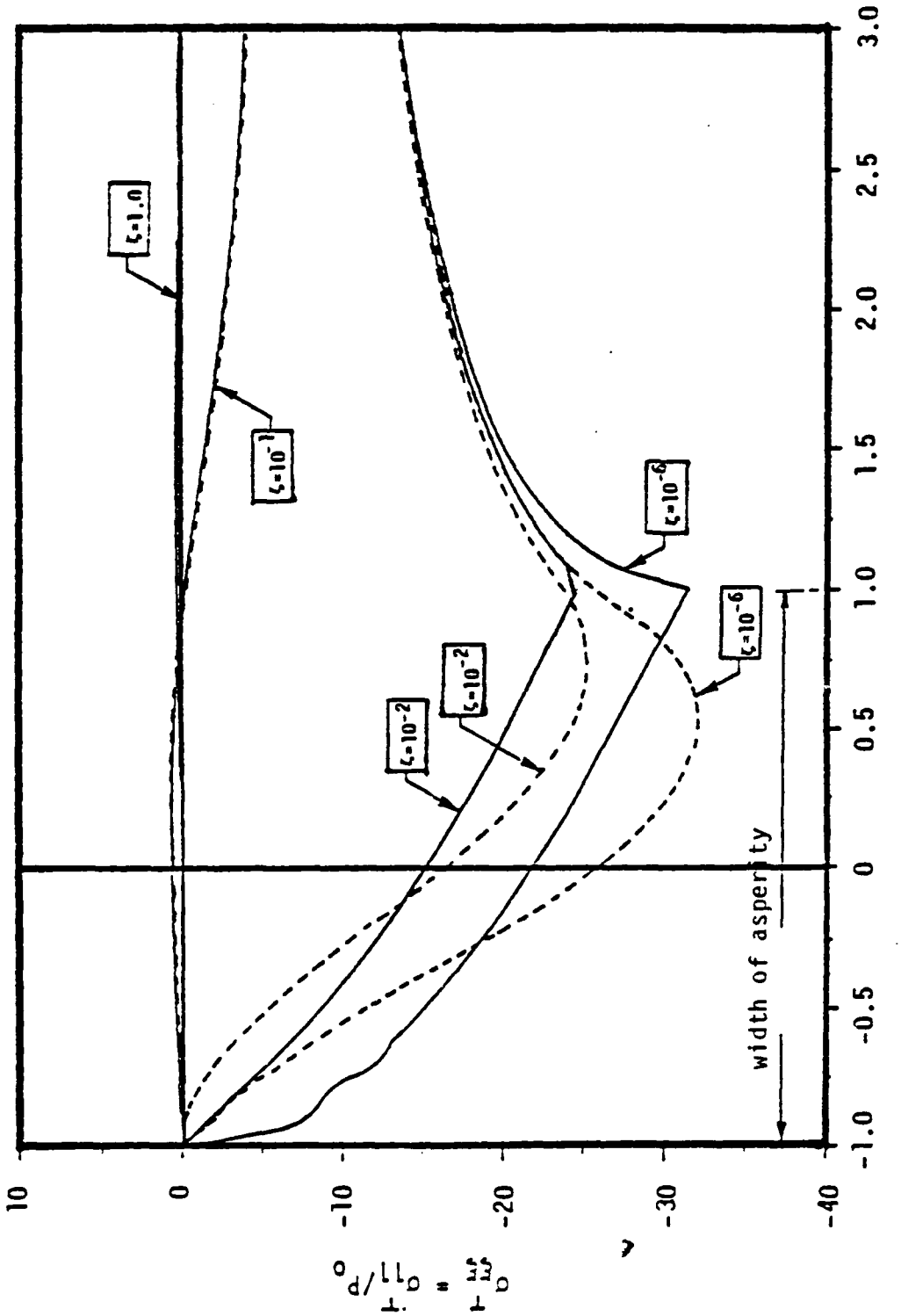

Figure. 2 Thermal stress at differnt depths in the neighborhood of or traversing asperity.

field near the surface layer as a result of high speed asperity traversing at 15 m/s (600 ips). The excessively high compressive stress at the surface layer indicates a plastic zone up to a depth of the order of 10 μm. The depth of plastic deformation is well of the same order for hard wear materials [9]. However, if the crack initiation due to cohesive failure occurs at a depth of an order of magnitude larger, the thermoelastic formulation of the thermomechanical cracking model in Art. 1.1 will hold. The maximum tensile stress due to thermal field will occur in the neighborhood of the depth of maximum temperature gradient. The temperature field and its gradient are respectively:

$$\phi(\xi,\eta,\zeta) = \int_0^\infty f(\xi,\eta,\theta)\, \exp(-\zeta^2/2\theta)d\theta, \tag{22}$$

$$\frac{d\phi}{d\zeta} = -\zeta \int_0^\infty \theta^{-1}\, f(\xi,\eta,\theta)\, \exp(-\zeta^2/2\theta)d\theta, \tag{23}$$

where $(\xi,\eta,\zeta) = (x_i/a)$ is the dimensionless coordinate, $\phi = Tk/q_0a$ is the dimensionless temperature field in the medium, q_0 is the heat flux due to the average frictional load, and

$$f(\xi,\eta,\theta) = \frac{1}{4\sqrt{2\pi\theta}}\left[\, \mathrm{erf}\left(\frac{\eta + t}{\sqrt{2\theta}}\right) - \mathrm{erf}\left(\frac{\eta - t}{\sqrt{2\theta}}\right)\right] \sum_{r=1}^{N} \left[\, \mathrm{erf}\left(\frac{\xi_r + 1}{\sqrt{2\theta}}\right) - \mathrm{erf}\left(\frac{\xi_r - 1}{\sqrt{2\theta}}\right)\right].$$

In the expression of $f(\xi,\eta,\theta)$, N is the number of repeated asperity excitations, t is the aspect ratio, $\xi_r = \xi - (r - 1)\lambda' - 1/2\ \mathrm{Pe}\ \theta$, λ' is the periodic length $V\tau/a$, τ is the period of excitation, $\mathrm{Pe} = Va/\kappa$ is the Peclet number. The expression is, without loss of generality, using a uniform load

distribution over a rectangular contact area. The depth (ζ_m), at which the maximum temperature gradient occurs, can be obtained by extremizing the temperature gradient, Equation (23), with respect to the depth ζ, such that

$$\left.\frac{d^2\phi}{d\zeta^2}\right|_{\zeta=\zeta_m} = \left.\int_0^\infty \theta^{-2}\,(\zeta^2 - \theta)\, f(\xi,\eta,\theta)\, \exp(-\zeta^2/2\theta)d\theta\right|_{\zeta=\zeta_m} = 0, \quad (24)$$

The maximum temperature-gradient occurs at a depth depending on the Peclet number, Pe, which is controlled by the asperity traversing speed (V) and the thermal diffusivity (κ). The solution to Equation (24) are obtained numerically for different values of number of asperity repetition (N), lateral position (η), contact area aspect ratio (t), and Peclet number (Pe). Figure 3 illustrates the depth of maximum temperature gradient in a hard wear material such as Stellite III as a function of the Peclet number for a single asperity, $\eta = 0$ and an aspect ratio of 10. The plot is up to some Peclet number corresponding to the magnitude of the traversing speed (V) in the neighborhood of the Rayleigh wave speed (c_R), beyond which the mathematical model no longer holds. It is noticed that up to Pe = 1.4×10^3 the depth ζ_m is fairly constant around 0.1. Based on the Stellite III as the medium, an asperity width of 0.5 mm (~0.02 in.) and a traversing speed of 15 m/s (~600 ips), result in Pe = 1200. The depth ζ_m thus defines the thermal layer near the wear surface. Since the layer is indeed by order of magnitude larger than the plastic layer, the mathematical model is justified.

The effect of the asperity traversing speed may thus be summarized as follows:

1. higher rate of frictional energy input, resulting in higher temperature, thus higher thermal stress,

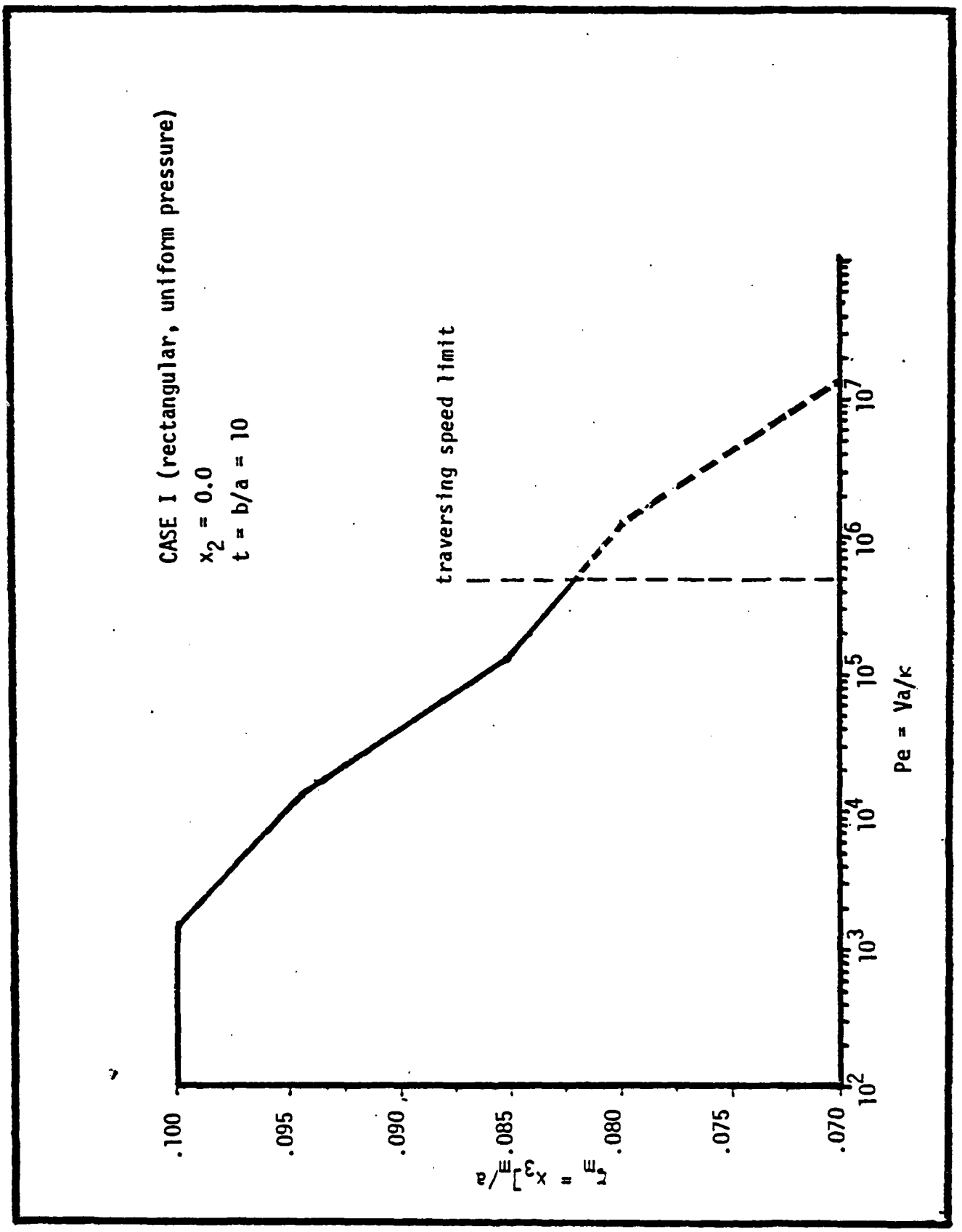

Figure 3. Depth of maximum temperature gradient vs Peclet no.

2. reduced thickness in thermal layer at higher speed, leading toward higher gradient thus higher thermal stress.

The dominance of thermal stress over the mechanical stress at high-speed asperity excitation (15 m/s) is shown in Figure 4. For a circular contact area with paraboloidal distribution of pressure and friction,

$$P(x_1,x_2) = P(r) = 2P_o\left(1 - \frac{r^2}{a^2}\right) \tag{22}$$

the thermal principal stress is six times higher than the mechanical principal stress. With uniform distribution of pressure the ratio is almost five times. The significance of the thermal components of the stress field cannot be overemphasized.

The load distribution in the contact area, taking into consideration of the thermo-mechanical behavior of the wear material, has not been determined either analytically or experimentally. With the result of Hertzian contact problem, the assumption of uniform distribution of loading is indeed an oversimplification. The analysis assumed a paraboloidal distribution with the same total load as the uniformly distributed load, Equation (22). The difference in the thermal principal stresses of the two is already evident in Figure 4. Figure 5 further compares the total thermomechanical principal stress of a paraboloidal distribution and a uniform distribution of loading in a circular contact area. For the same total asperity loading, the assumption of a paraboloidal distribution would result in a thermo-mechanical principal stress around 80% higher than that resulted from the assumption of uniform distribution. Of course neither may claim to be the true distribution of load in the asperity contact area. But the one of paraboloidal distribution does give a conservective estimate of crack initiation and may very well be closer to the real distribution of load.

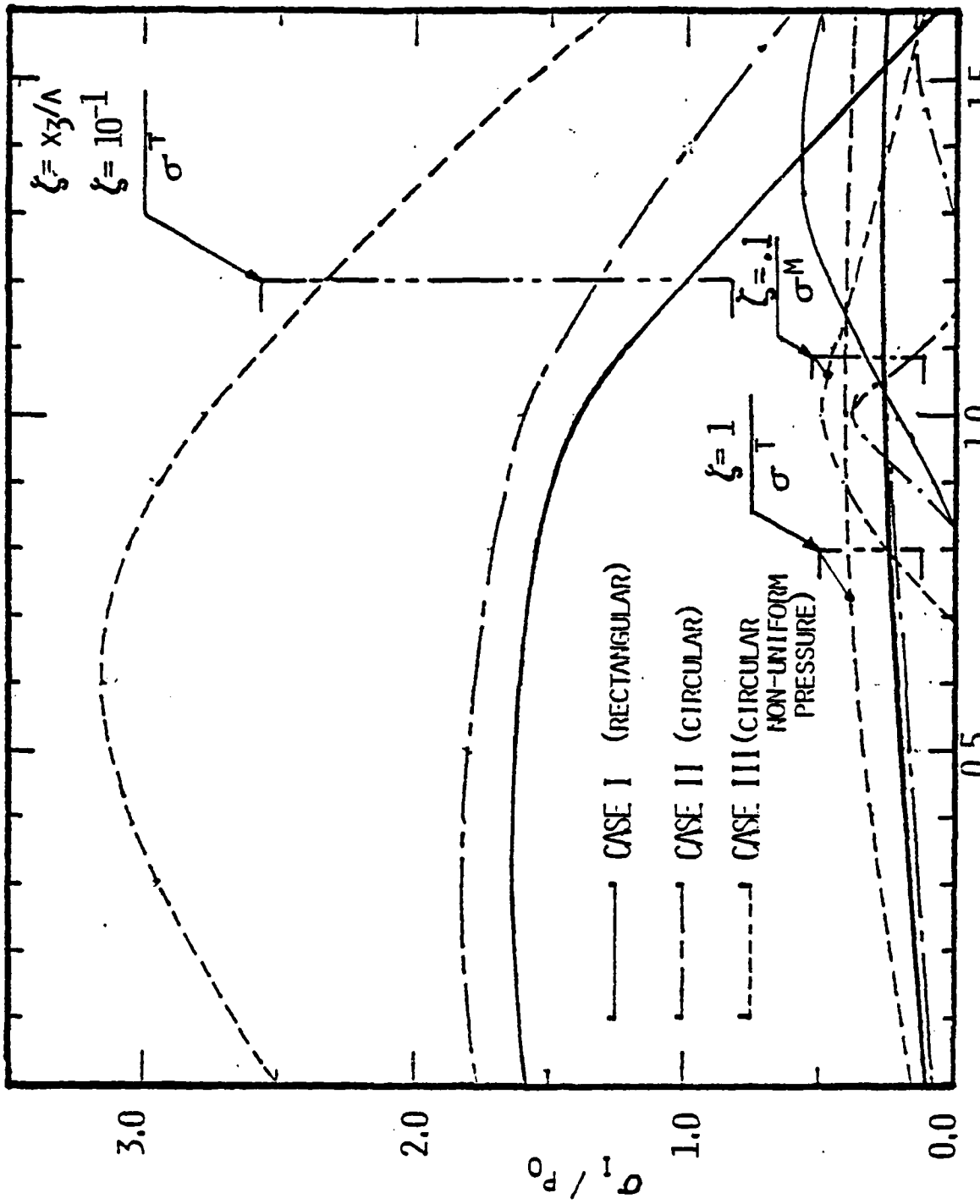

Figure 4. Comparison of thermal and mechanical stresses.

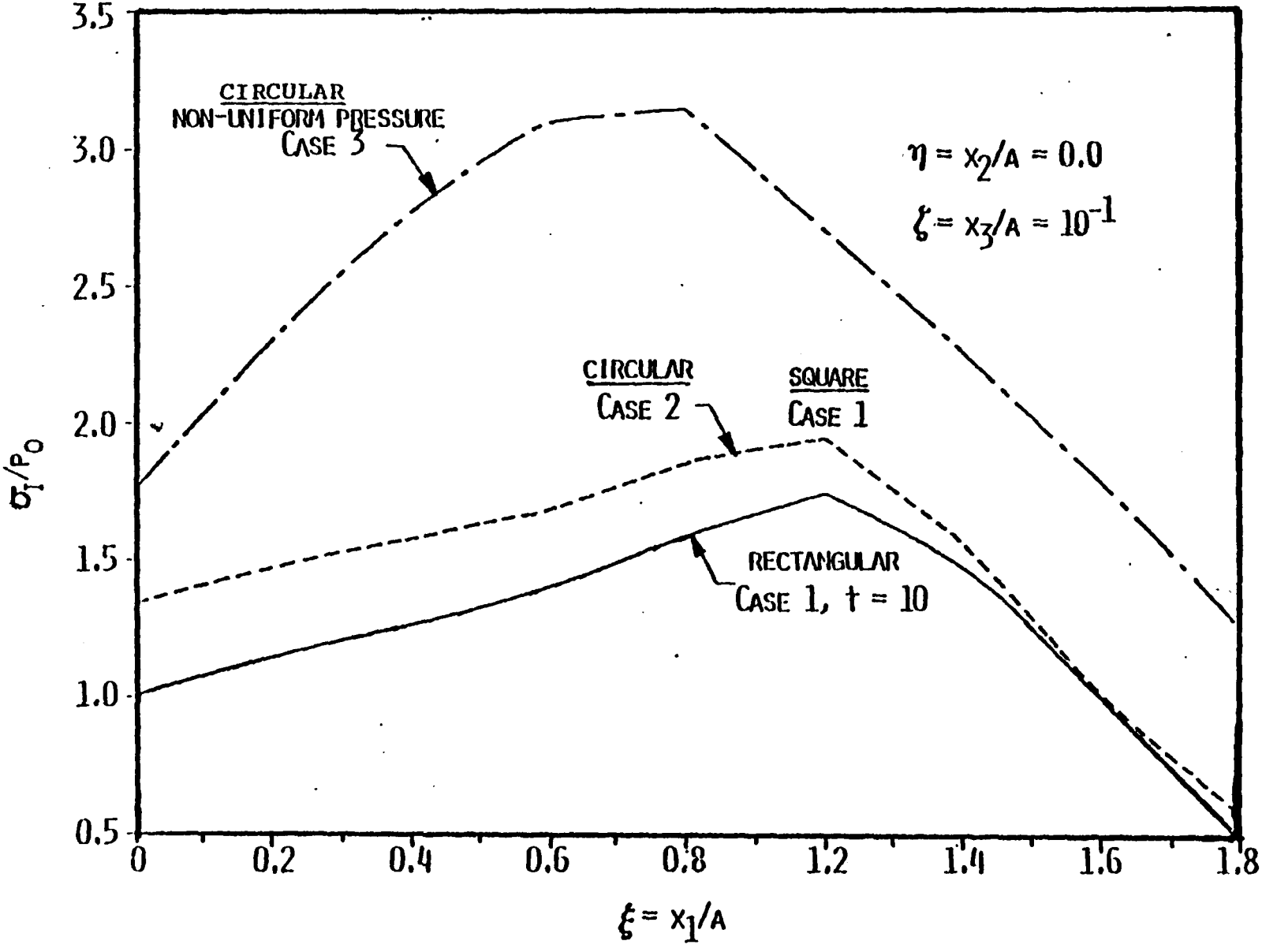

Figure 5. Stress fields for varying contact area and load distribution.

2.2 Contact Area Parameters

The study considers both the shape of the contact area and the aspect ratio of the contact area. Since the actual integral must be carried out numerically, it is difficult to generate a theory for all contact area shapes. For practical purpose and computation feasibility, the thermo-mechanical principal stresses of a circular and a square contact areas will be compared. There is very little noticeable difference; that is, the differences are less than the permissible numerical errors. It is therefore postulated that the shape of the contact area is not essential in wear analysis of asperity excitation.

The effect of the aspect ratio (t) of the contact area covers the study or a square (or circular, $t = 1$) area ranging toward a line contact ($t = \infty$), where the problem would be reduced to two-dimensional. Figure 6 shows the consistent trend of lower stresses with increase in aspect ratios. To the limit is the two-dimensionl ($t = \infty$) solution, of which the value is only one-sixth of the three-dimensional solution of stresses.

It is to be emphasized that the two-dimensional and the three-dimensional solutions of stresses from the mechanical loading portion are essentially the same. Hence, the phenomenon is principally thermal. Indeed, both the two-dimensional and the three-dimensional theories predict approximately the same surface temperature. But the three-dimensional model, because of the lateral (perpendicular to the plane) heat loss, will drop temperature more rapidly thus higher temperature gradient, leading toward higher thermal stresses.

The effects from different half-widths are shown in Figure 7. It is noted that higher solutions result from larger asperity size which leads to more heat input, thus higher temperature gradient. However, larger width implies larger contact area with correspondingly reduced pressure. The

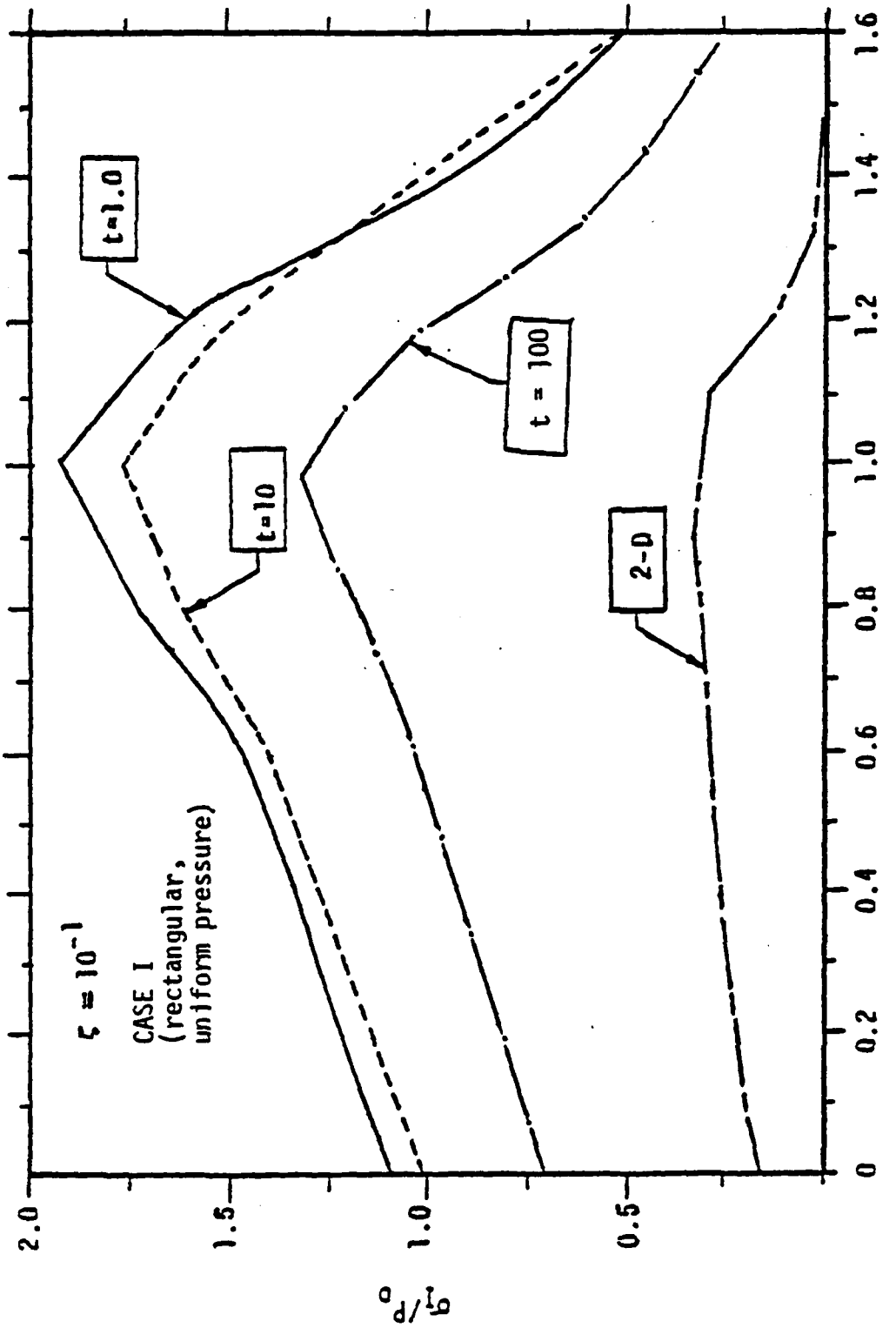

Figure 6. Stress field corresponding to varying aspect ratio.

increasing stress with the increase of half-width (a) is less than linear, which may be observed in Figure 7; while the decrease in pressure is most likely inversely proportional to the square of the characteristic dimension (a). The result is definitely beneficial for larger a, if it is design controllable.

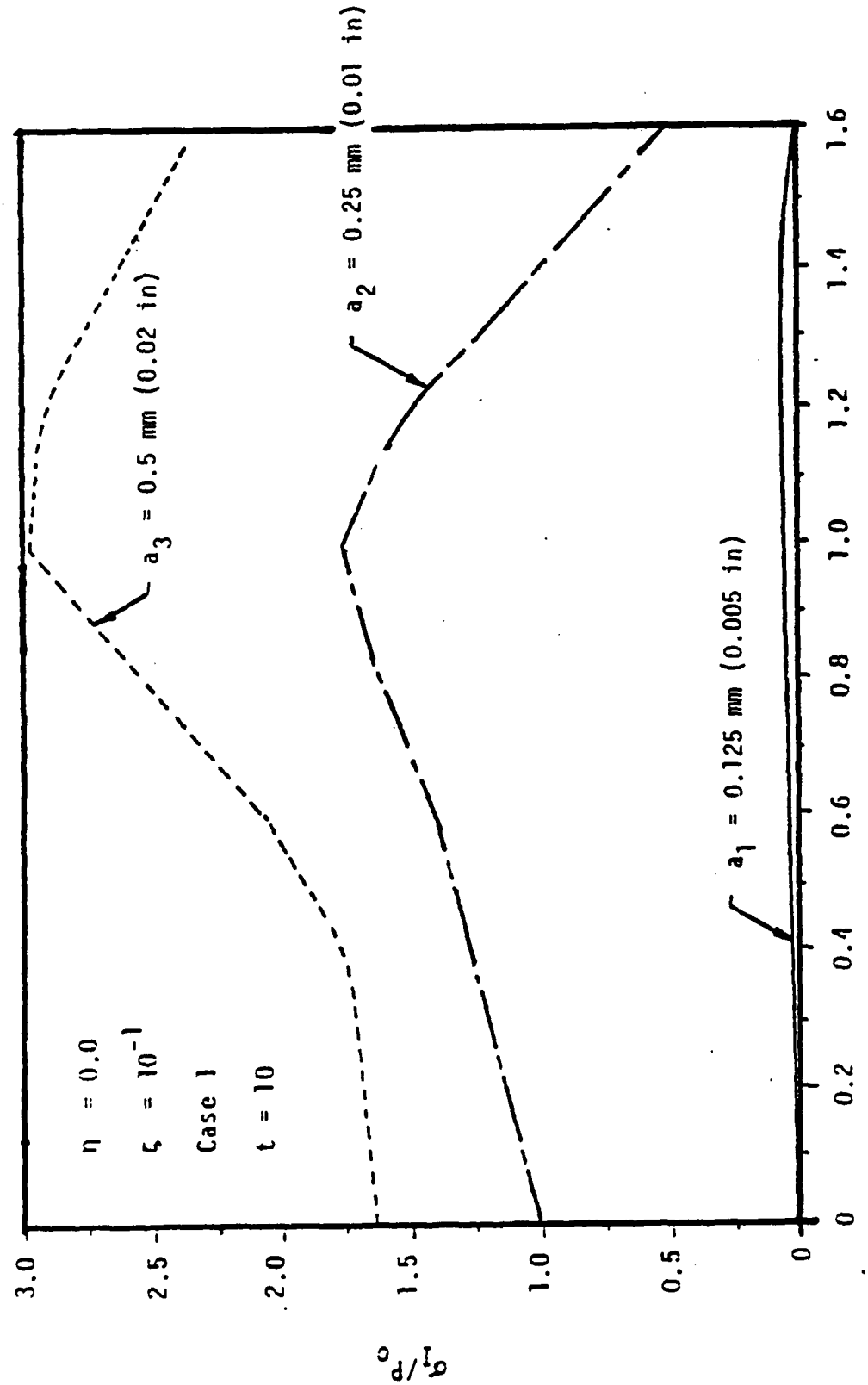

Figure 7. Asperity width effect.

3.0 MATERIAL PROPERTY PARAMETERS

The material parameters under consideration are the mechanical constitutive coefficients (λ,μ) or (E,ν), respectively the Lame's coefficients and the pair of Young's Modulus and Poisson's Ratio, and the mass density (ρ), the coefficient of Coulomb friction (μ_f), the coefficient of thermal expansion (α), the thermal diffusivity (κ) and the thermal conductivity (k). Their effects are mostly thermal. The mechanical portion, as a result of tractions only, is essentially related to the prescribed loads. For the problem of the current asperity speed, it is the thermal component that dominates the thermomechanical cracking phenomenon. In order to keep the mathematics manageable, some simplified postulations are necessary. For instance, the report adopts the simple Coulomb's law on the friction force, $F_f = \mu_f F_n$. The heating effect of the friction force influences in the surface layer a temperature rise, which in turn increases the Coulomb coefficient μ_f with resulting further increase in friction force [2]. The analysis, therefore, avoids the iteration by presuming a relatively high constant coefficient to anticipate a steady state high temperature field. The numerical computation of thermal stresses is thus based on a coefficient of Coulomb friction of 0.5, which is conservative for high coefficient of friction. The mass density (ρ) affects the mechanical portion of the stress field, Equation (18), through the Mach numbers (M_r) and the thermal field through the thermal diffusivity $(\kappa = k/\rho c)$. Since the Mach number is generally small in this class of problems and the mechanical portion of the stress field is less significant, the effect of the mass density is principally combined with the specific heat (c) to define the thermal capacity (ρc) in affecting the value of the thermal diffusivity (κ).

3.1 Mechanical Properties

It is noticed in the thermal stress equation (21) and the definitions of the coefficients $\{b_i\}$ that the thermal stresses are directly proportional to its stiffness (μ or E) -- modulus of rigidity or Young's modulus, and the coefficient of thermal expansion α (as a factor in the coefficient a_3). The effect of the Poisson's ratio is rather obscure. Figure 8 illustrates the fact that materials with five times difference in stiffness does indeed show corresponding difference in the maximum principal stress. The variance of the Poisson's ratio, which is usually around 0.3, does not indicate to be a significant factor. Yet, as shown in Figure 8, the principal stress will increase slightly with increase in the Poisson's ratio. It is also noticed that, even though the mechanical portion of the stress components are independent of the material stiffness, Equation (18), the effect of stiffness on the combined thermomechanical principal stress is still significant, owing to the dominance of the thermal effect in high speed asperity excitation.

3.2 Thermal Properties

Similar to the effect of stiffness of the wear material, the mechanical portion of stresses is also independent of the coefficient of thermal expansion. But the combined thermomechanical stress is almost directly proportional to the coefficient of thermal expansion as indicated in Figure 9. Physically it is apparent that higher coefficient of thermal expansion introduces more mechanical constraint in the material for the same temperature gradient.

The effect of the thermal diffusivity (κ) is more complex. Although the thermal diffusivity occurs as the only thermal property apparent in the governing differential equation (5), its value is determined by the coeffi-

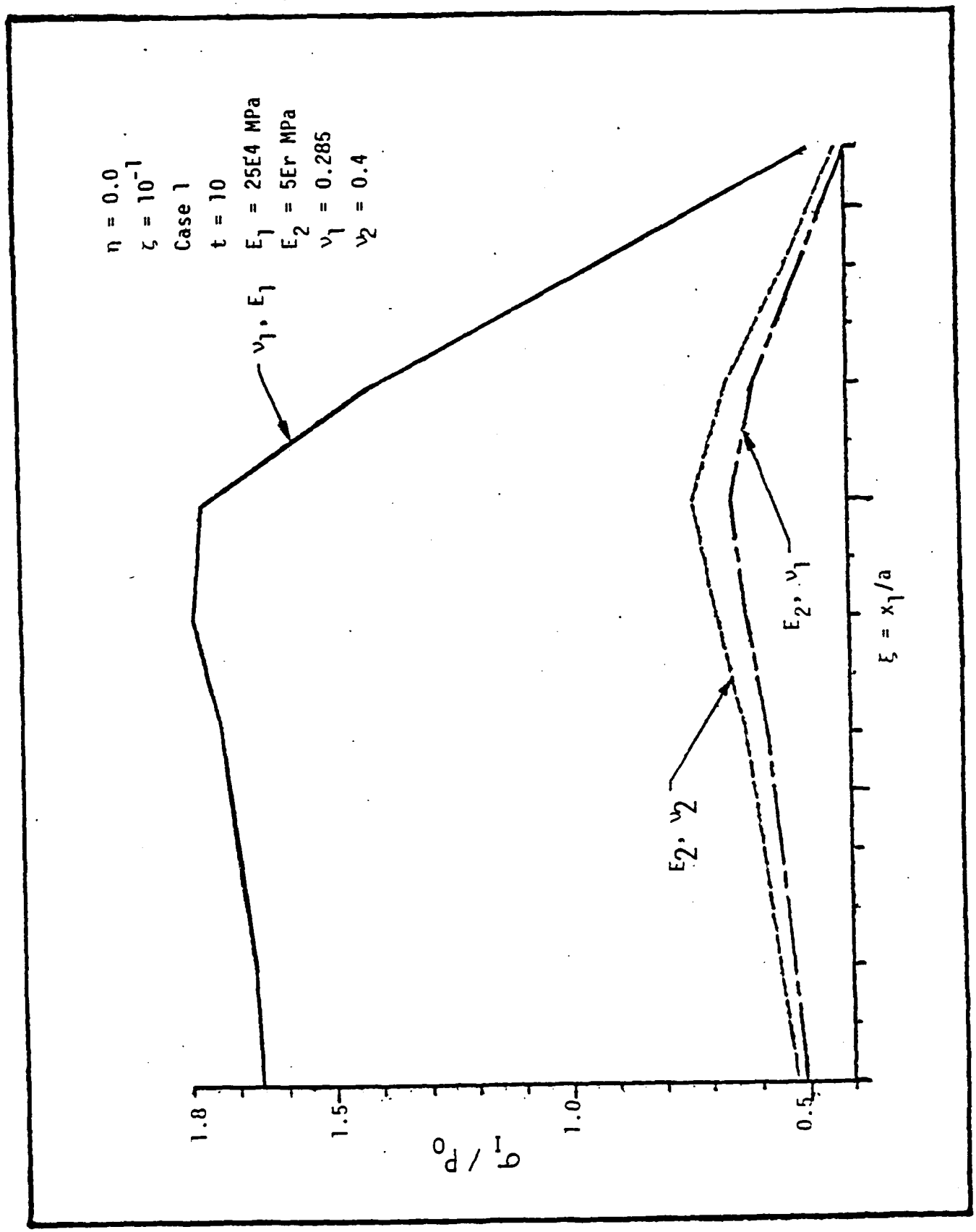

Figure 8. Stiffness effect on the stress field.

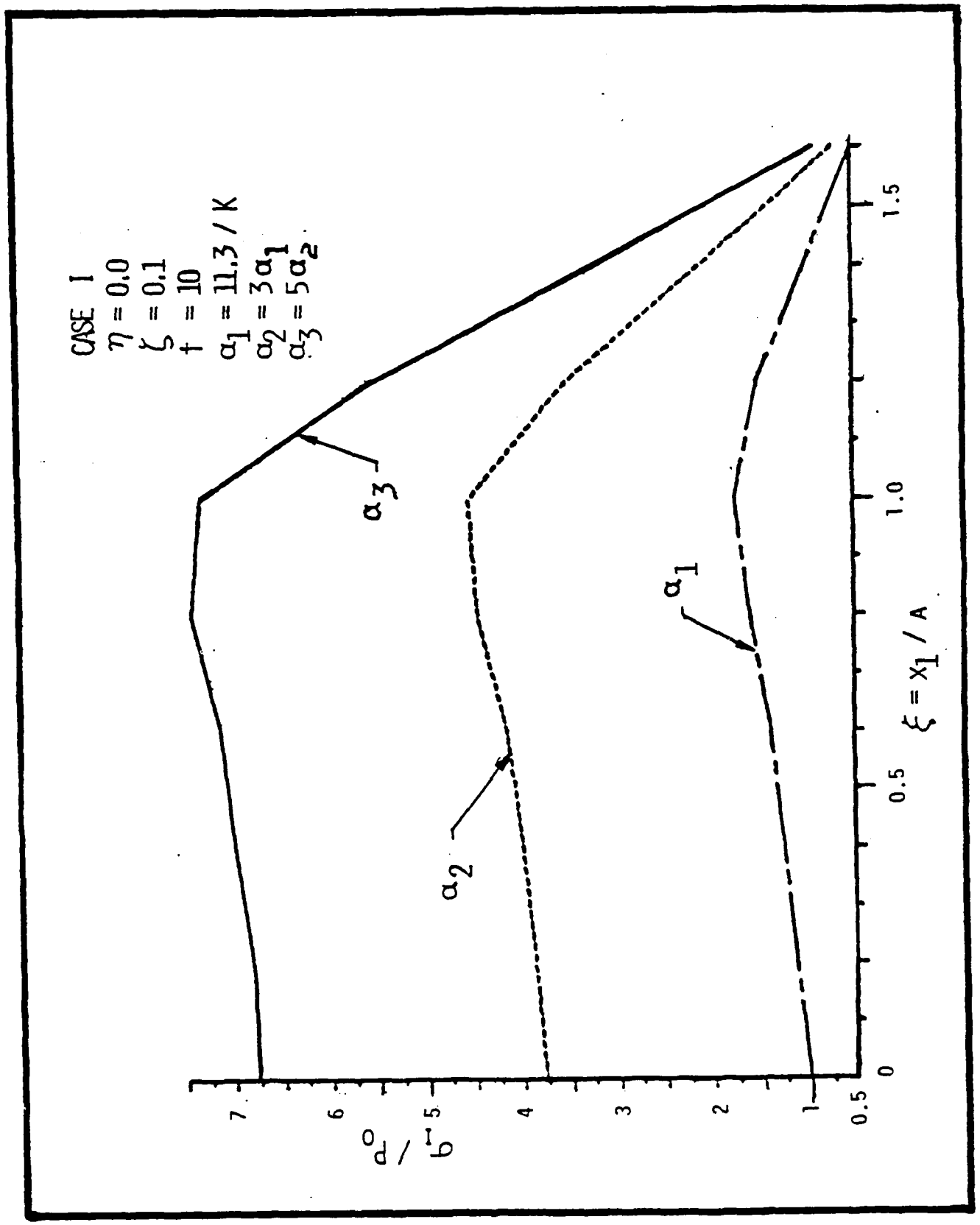

Figure 9. Effect of coefficient of thermal expansion on the stress field.

cient of thermal conductivity (k) and the thermal capacity (ρc) in that $\kappa = k/\rho c$. If the thermal conductivity (k) is kept constant, the lowering of thermal diffusivity will lower the temperature field because of increase in the thermal capacity (ρc). It lowers the temperature field; and its effect on the thermal stress, is positive. However, if the reduction in the thermal diffusivity is caused by a reduction in thermal conductivity (k), the boundary condition (Equation 17) is also affected, resulting in higher temperature gradient thus higher thermal stress. Figure 10 illustrates the case for which the thermal capacity (ρc) remains constant. The change in the thermal diffusivity is directly proportional to the change in the thermal conductivity. The maximum principal stress increases with decrease of the thermal conductivity, thus thermal diffusivity, even though not exactly in inverse proportion. However, if the reduction in the thermal diffusivity is due to the increase in thermal capacity rather than the decrease in thermal conductivity, lower stress will result. The effects of variation in thermal properties on the maximum thermal stress at the depth $\zeta = 0.1$ for a uniformly loaded rectangular contact area $t = 10$ and an asperity speed of 15 m/s, is illustrated in Figure 11. Curves 1 through 3 maintain a constant thermal capacity. Curve 1 uses the thermal properties of Stellite III. Curves 2 and 3 illustrate the decrease and increase of the principal thermal stresses corresponding to the doubling or halving the thermal diffusivity. However, when the halving of the thermal diffusivity is caused by a doubling in the thermal capacity rather than halving of the thermal conductivity, the principal thermal stress reduces almost in half as shown by Curve 4. Finally, as significantly illustrated in Curve 5, the thermal diffusivity is kept the same as in Curve 1, but both the thermal conductivity and the thermal capacity are halved. The ensuing increase in thermal stress is most noticeable.

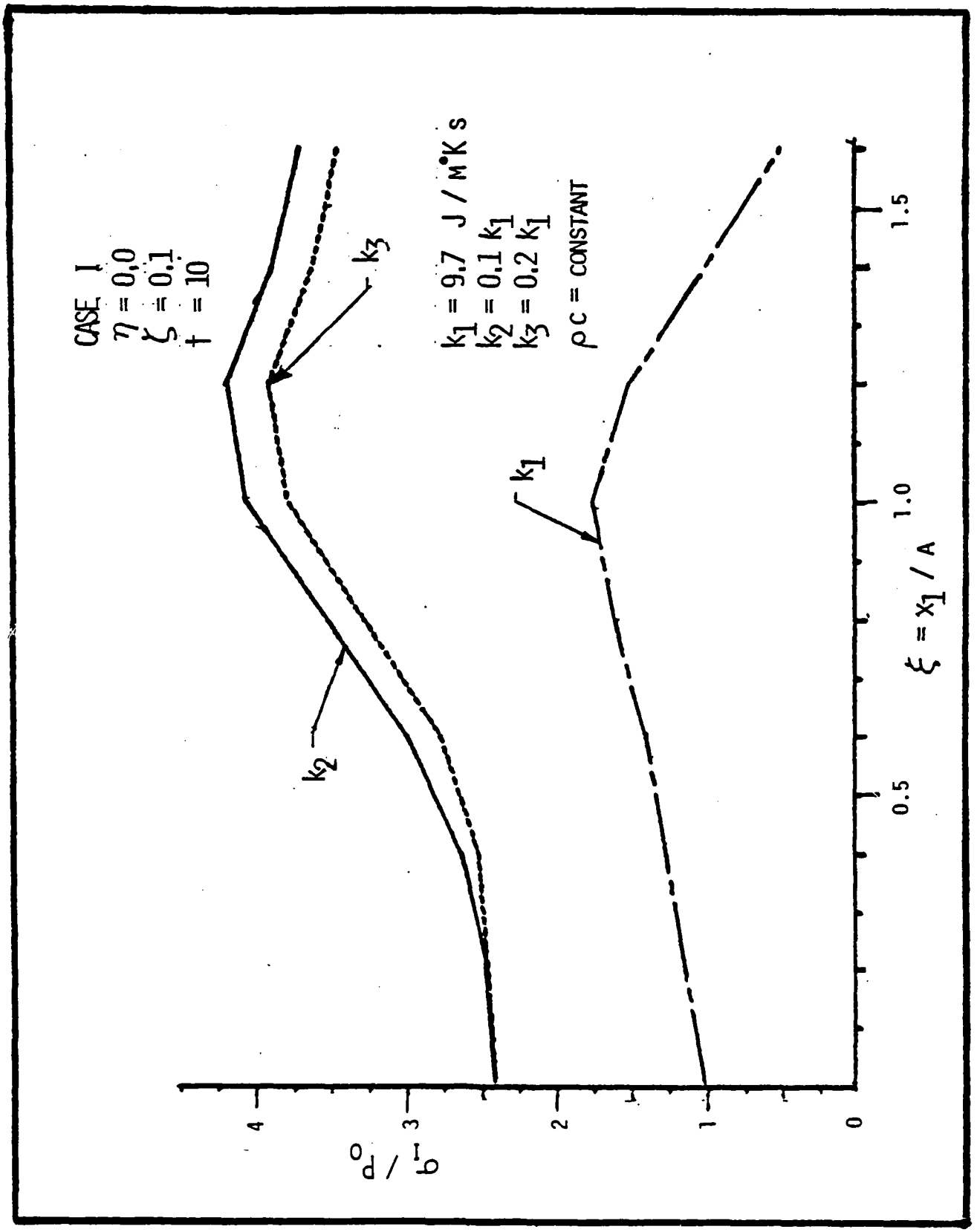

Figure 10. Effect of thermal conductivity on the stress field.

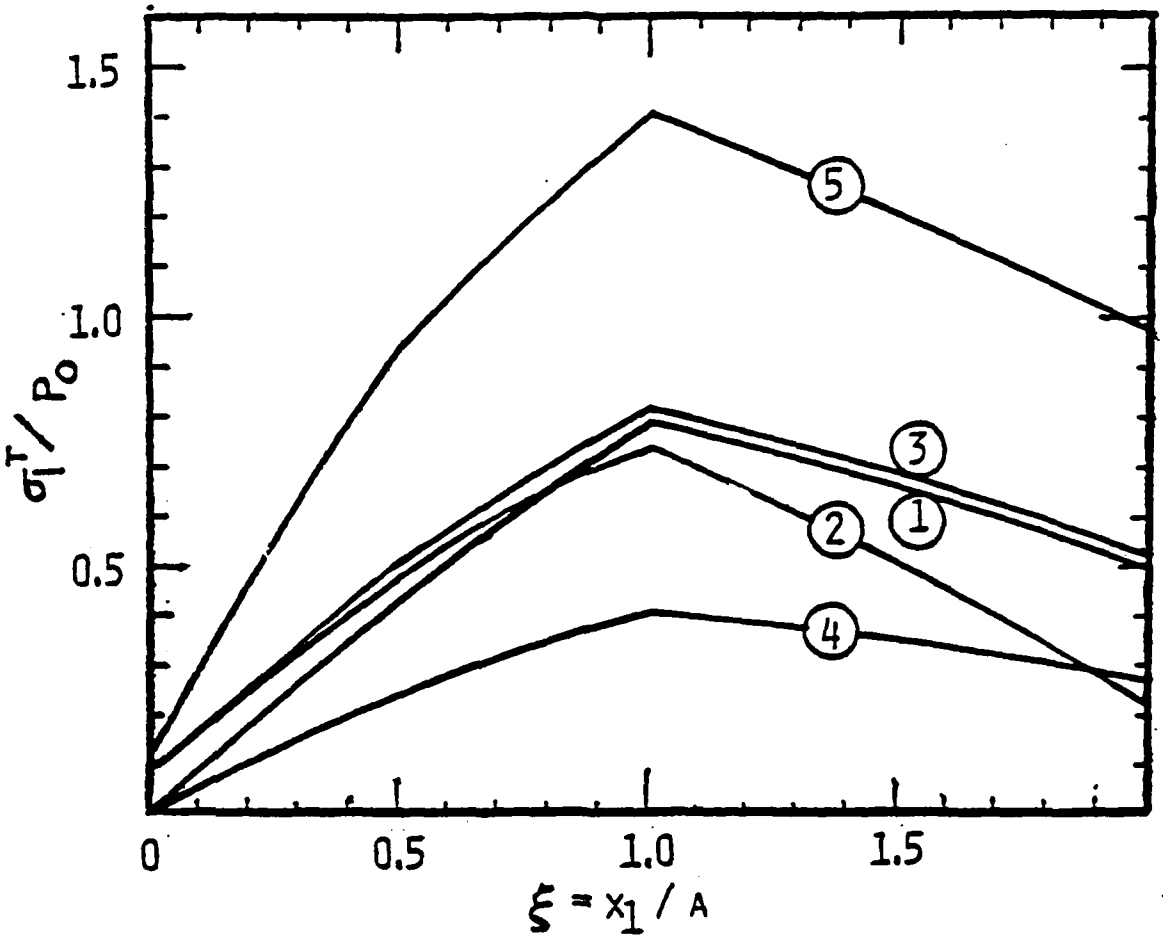

1. $\kappa_1 = \kappa$, $k_1 = k$, $c_1 = c$
2. $\kappa_2 = 2\kappa$, $k_2 = 2k$, $c_2 = c$
3. $\kappa_3 = \kappa / 2$, $k_3 = k / 2$, $c_3 = c$
4. $\kappa_4 = \kappa / 2$; $k_4 = k$, $c_4 = 2c$
5. $\kappa_5 = \kappa$, $k_5 = k / 2$, $c_5 = c / 2$

Fig. 11. Effect of variation in thermal properties.

4.0 CONCLUSION

The parametric study enhances the understanding or thermomechanical cracking through the mechanism of subsurface cohesive failure, which is predominantly a thermal stress phenomenon at high speed asperity excitation. The asperity parameters are, in general, not controllable quantities. The purpose is therefore to improve analysis for conservative designs. For instance, a parabolic distribution, resulting in higher themomechanical stress, is preferred over the assumption of uniform distribution. The asperity initiated cracking is essentially a three-dimensional phenomenon; two-dimensional analysis under-estimated stress level by six times. The use of uniform load distribution and two-dimensional formulation cannot be justified for actual design computation unless an artificial and high factor of safety is used. Their use may be used in cases:

1. Two-dimensional theory yields the same mechanical stress field and the same surface temperature as those from the three-dimensional theory developed in [6,7]. In such case, two-dimension theory may be preferred for its much simpler mathematical computation.

2. Uniform distribution of load may be employed for the illustration of parametric effect in the comparison of stress magnitudes. Since the relative stress levels rather than the real ones are of interest, the simplification in mathematical analysis is justified.

The other non-controllable asperity parameter is the asperity shape. It is gratifying with the demonstration of the comparison of a square and a circular contact area, both of an aspect ratio of $t = 1$, that the difference of their results is negligibly small. The asperity speed affects the thermomechanical field two-fold. In one, the higher speed results in a higher heat input, VR_1, leading toward a higher thermal stress field. In another,

the higher speed increases the Peclet number, causing a decrease of the thermal layer, the distance between the wear surface and the depth of maximum temperature gradient. This decrease in the thermal layer, itself would cause an increase in the temperature gradient, thus promoting an increase in the thermal stress.

Among the material properties, the stiffness (μ or E) and the coefficient of thermal expansion (α) are directly proportional to the principal thermal stress. They are unrelated to the mechanical portion of the stress field. In view of the predominance of thermal stress field for high speed asperity excitation, the choice of stiffer wear material must be compensated by a sufficient reduction in the coefficient of Coulomb friction.

The thermal properties to be considered in design should be the thermal conductivity (k) and the thermal capacity (ρc). The thermal diffusivity is a derivative parameter. High thermal conductivity and high thermal capacity are definitely preferred to reduce the thermal stress. Furthermore, an increase in thermal conductivity would lead to lower Peclet number ($Pe = V\ell/\kappa$) thus thicker thermal layer. The ensuing reduction in temperature gradient will result in a further decrease in the thermal stress field.

The present report thus identifies those parameters to be considered in analysis and in design. The information should assist the analyst to choose the proper mathematical model and the designer to select wear materials based on the influential material properties for an optimal design.

REFERENCES

1. Greenwood, J.A. and Williamson, J.B., "Contact of Nominally Flat Surfaces," Proc. Royal Soc. London, Ser. A, v. 295, 1966, p. 300.

2. Burton, R.A., "Friction and Wear," Chap. 2, Tribology, ed. A.Z. Szeri, McGraw-Hill, 1980, pp. 17-38.

3. Archard, J.F., "The Temperature of Rubbing Surfaces," Wear, v. 2, 6, 1959, pp. 438-455.

4. Burton, R.A., "Thermomechanical Effects in Sliding Ware," Workshop on Frictionally Induced Thermal Deformation and Ware, Annapolis, MD, June 19-20, 1979.

5. Kennedy, F.E. and Karpe, S.L., "Thermocracking of a Mechanical Face Seal," Wear, 79, 1982, pp. 21-36.

6. Ju, F.D. and Huang, J.H., "Thermomechanical Cracking Due to Moving Friction Loads," UNM Report No. ME-125(84)ONR-233-2, May 1984.

7. Huang, J.H. and Ju, F.D., "Thermomechanical Cracking Due to Moving Friction Load -- Part II. A Three Diminsional Model of a Single Asperity," Wear, v. 102, 1985, pp. 87-97.

8. Carslaw, H.S. and Jaeger, J.C., Conduction of Heat in Solids, 2nd ed., Clarendon Press, Oxford, 1959.

9. Blau, P.J., "The Role of Metallurgical Structure in the Integrity of Sliding Solid Contacts," Solid Contact and Lubrication, ASME AMD-v. 39, 1980, pp. 185-191.

10. Ruff, A.W. and Blau, P.J., Studies of Microscopic Aspects of Wear Processes in Metals, National Bureau of Std. NBSIR 80-2058, June 1980.

END

DTIC

8-86